

The three-dimensional behavior of inverted pendulum cylindrical structures during earthquakes

Michalis F. Vassiliou^{*,†} , Stefan Burger, Marius Egger, Jonas A. Bachmann ,
Marco Broccardo and Bozidar Stojadinovic

*Institute of Structural Engineering (IBK), Department of Civil, Environmental, and Geomatic Engineering (BAUG),
Swiss Federal Institute of Technology (ETHZ), Stefano-Francini-Platz 5, 8093 Zürich, Switzerland*

SUMMARY

In order to use rocking as a seismic response modification strategy along both directions of seismic excitation, a three-dimensional (3D) rocking model should be developed. Since stepping or rolling rocking structural members out of their initial position is not a desirable performance, a rocking design should not involve these modes of motion. To this end, a model that takes the aforementioned constraint into account needs to be developed. This paper examines the 3D motion of a bounded rigid cylinder that is allowed to uplift and sustain rocking and wobbling (unsteady rolling) motion without sliding or rolling out of its initial position (i.e., a 3D inverted pendulum). Thus, the cylinder is constrained to zero residual displacement at the end of its 3D motion. This 3D dynamic model of the rocking rigid cylinder has two DOFs (three when damping is included), making it the simplest 3D extension of Housner's classical two-dimensional (2D) rocking model. The development of models with and without damping is presented first. They are simple enough to perform extensive parametric analyses. Modes of motion of the cylinder are identified and presented. Then, 3D rocking and wobbling earthquake response spectra are constructed and compared with the classical 2D rocking earthquake response spectra. The 3D bounded rocking earthquake response spectra for the ground motions considered seem to have a very simple linear form. Finally, it is shown that the use of a 2D rocking model may lead to unacceptably unconservative estimates of the 3D rocking and wobbling seismic response. Copyright © 2017 John Wiley & Sons, Ltd.

Received 24 November 2016; Revised 7 March 2017; Accepted 7 March 2017

KEY WORDS: rocking isolation; 3D rocking motion; uplifting structures; wobbling; rolling

1. INTRODUCTION

To the authors' knowledge, the first modern interest in rocking structures stemmed from the need to estimate the peak acceleration of ground motions by studying overturned blocks. In 1885, Milne [1] published a study that hinges upon the assumption that the uplifting acceleration of a rigid block is enough to overturn it. In 1927, in an effort to construct an acceleration measuring device, Kirkpatrick [2] uncovered that the overturning of a block does not only depend on the ground motion peak ground acceleration (PGA) and on the block slenderness but also on the ground motion duration and the block size. In 1963, Housner [3] published his seminal paper where he explained the remarkable properties of rocking structures: (i) the larger of two geometrically similar blocks can survive the excitation that will topple the smaller block, and (ii) out of two acceleration pulses with the same acceleration amplitude, the one with longer duration is more capable of inducing

*Correspondence to: Michalis F. Vassiliou, Institute of Structural Engineering (IBK), Department of Civil, Environmental and Geomatic Engineering (BAUG), Swiss Federal Institute of Technology (ETHZ), Stefano-Francini-Platz 5, 8093 Zürich, Switzerland.

†E-mail: mfvassiliou@gmail.com

overturning. These properties, as well as the observation that modern and ancient structures that were unintentionally designed to rock behaved well during earthquakes, have motivated engineers to try to use uplifting of structures as a seismic response modification strategy.

The behavior of a simple, free-standing rigid rocking block has been systematically studied for more than three decades [4–16]. The behavior of deformable solitary rocking oscillators has also been studied [17–21], and it was concluded that deformable rocking structures also present remarkable stability when excited by earthquakes. This favorable property is also present in the dynamic behavior of assemblies or rocking bodies, such as multidrum ancient columns [22] or rocking frames or walls [23–28]. Experiments show that the deterministic models of impact damping are not easy to validate [18, 29–31], thus necessitating a probabilistic treatment [32–34]. Models to quantify the effects of the prestressing tendons [35, 36] or viscous dampers [37] added to rocking blocks and rocking frames have also been proposed.

All of the aforementioned works treat rocking as a 2D, in-plane, problem. The published research on the dynamic response of 3D rocking of rigid bodies is much more limited. In [38–40], the motion of a rigid cylinder under seismic excitation is studied. Other researchers studied the 3D response of ancient conical or cylindrical columns numerically [41, 42] or experimentally [43–45]. Makris *et al.* [46] experimentally tested scaled models of uplifting bridges. All the aforementioned studies conclude that 3D motion is present (so-called wobbling), even under in-plane initial conditions and/or under uniaxial horizontal component ground excitation. Stefanou *et al.* [47] proved the aforementioned observation theoretically. In fact, when the initial spin tends to zero, the motion of a rigid cylinder involves a sudden and rapid motion of the contact point around the circular base (wobbling) instead of an impact (rocking). Srinivasian and Ruina [48] proved that the net angle of turn of the contact point is nearly independent of initial conditions: instead, this angle of turn depends simply on the geometry and the mass distribution of the body.

Beyond the scope of earthquake engineering, Moffat [49] described the motion of a toy, the ‘Euler’s Disk’ (which is not related to Euler but is named after the Euler angles used to describe its motion). The toy comprises a disk that is given an initial spin on a chromed concave base. The toy spins with an increasing frequency and stops in an abrupt manner. Similar behavior is observed when spinning a coin. Even though there is no evident engineering application of the toy, Moffat’s paper received much attention and created a debate about the energy dissipation mechanisms involved in the motion of Euler’s Disk [50–53].

The 3D behavior of non-cylindrical bodies has also recently received attention. Konstantinidis and Makris [54] and Zulli *et al.* [55] studied the rocking motion of a 3D prism. Chatzis and Smyth [56] studied the motion of a 3D prism on a deformable base, taking sliding into account as well as the 3D dynamics of a rigid body with wheels on a moving base [57]. Greenbaum [58] developed an interesting computer vision method that allows for the experimental measurement of the rigid-body translation and rotation time histories in three dimensions. Mathey *et al.* [59] studied the influence of geometric defects on the 3D response of small-sized blocks. They concluded that the blocks with imperfections are less stable than the theoretically perfect ones. Pappas *et al.* [60] numerically explored the behavior of an ancient cylindrical column with a height of 6 m and a diameter of 0.66 m with the intention of defining proper ground motion intensity measures to characterize the rocking response of such structures.

Dynamic models used in the research discussed earlier are multi-degree-of-freedom (MDOF) models and assume unbounded 3D motion. They involve stepping or rolling rigid rocking bodies out of their initial position. This behavior results to residual deformations. Thus, these models are suitable for equipment but not for structural components designed to uplift. In contrast, a simpler model is examined in this paper: a cylinder rocking and wobbling (rolling unsteadily) exclusively above the initial position of its base, without sliding or rolling out (i.e., a 3D inverted pendulum). In this sense, the investigated model is a direct extension of Housner’s model, which also constrains the rocking body to restore to its original position. This simplified 3D bounded rocking and wobbling motion model is developed because, if rocking is to be used for seismic response modification, no residual displacement or rolling out of the body would be acceptable. Such motion constraints could be implemented, for example, as a recess around the cylindrical column or via methods presented in [61]. The accuracy of the model depends on how efficiently the constraints are

implemented. The model investigated herein is much simpler and computationally cheaper than the MDOF models, thereby allowing for extensive parametric studies and probabilistic seismic analysis. Two versions of the model are developed and compared: one without and the other with damping.

2. UNDAMPED 3D BOUNDED MODEL OF A FREE-STANDING RIGID CYLINDER

2.1. Coordinate systems

The 3D bounded rocking and wobbling model of a free-standing rigid cylinder is shown in Figure 1. The cylinder has a total mass, m ; base radius, b ; and height, $2h$. Its semidiagonal is R , and its slenderness is α ($\tan\alpha = b/h$). The assumptions are as follows:

1. The cylinder is considered rigid, homogeneous, and not damageable.
2. The supporting plane surface (ground) is considered rigid and not damageable.
3. The contact between the cylinder and the ground is pointwise. This assumption becomes more accurate for smaller cylinders and for larger tilt angles.
4. The cylinder is constrained not to roll out of its initial position.
5. No sliding is allowed; that is, the friction between the cylinder and the supporting plane surface is assumed to be large enough.

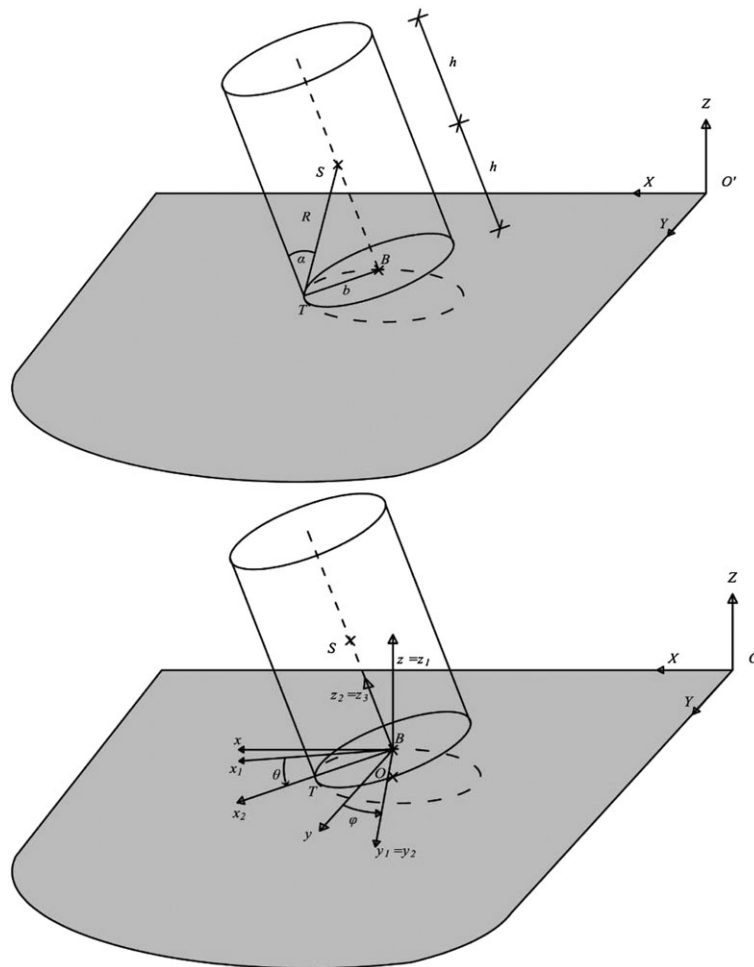


Figure 1. Top: geometry of the model. A rigid cylinder is allowed to uplift and wobble but is constrained not to roll out of its original base. Bottom: ‘3–2–3’ Euler angles.

6. The cylinder is always in contact with the support (i.e., it never flies). Therefore, the contact force is always compressive.
7. No damping mechanism is included.

Given the aforementioned assumptions, the model has only two degrees of freedom: the tilt angle, θ , and the rolling angle, φ . The latter determines the location of the contact point between the cylinder and the supporting plane (Figure 2).

The following coordinate systems are used (Figure 1, bottom): XYZ is the inertial reference frame; xyz originates at the center of the bottom of the cylinder, B , and has the same orientation as XYZ ; $x_3y_3z_3$ originates at B and follows the rotations of the cylinder. At rest, all three coordinate systems have the same orientation, and the last two coincide.

Coordinate systems XYZ and xyz differ only by a translation; system $x_3y_3z_3$ is a rotation of xyz . The so-called 3–2–3 Euler angles are used to describe this rotation [62]. The first angle (notated as φ , since it can be proven that it is equal to the rolling angle) describes a rotation around the axis z . This leads to a new coordinate system $x_1y_1z_1$. The second angle (notated as θ , since it can be proven that it is equal to the cylinder tilt angle) describes a rotation around the axis y_1 . This leads to the new coordinate system $x_2y_2z_2$. The third angle, ψ , describes a rotation around the axis y_2 . This leads to the new coordinate system $x_3y_3z_3$. Since it is assumed that the friction between the cylinder and the foundation is large, it can be proven that $\psi = -\varphi$.

In order to derive the equation of motion of the cylinder, the translational and rotational motions of the center of mass of the cylinder should be tracked, relative to the inertial reference frame XYZ . Referring to Figure 2, the position vector of the center of mass, S , is as follows:

$$\mathbf{r}_{O'S} = \mathbf{r}_{O'O} + \mathbf{r}_{OB} + \mathbf{r}_{BS} \tag{1}$$

The components of the position vector are as follows (Figure 2):

$$\mathbf{r}_{O'O} = u_{ox}\mathbf{I} + u_{oy}\mathbf{J} + 0\mathbf{K} \tag{2}$$

$$\mathbf{r}_{OB} = d_x\mathbf{i} + d_y\mathbf{j} + d_z\mathbf{k} \tag{3}$$

$$\mathbf{r}_{BS} = 0\mathbf{i}_3 + 0\mathbf{j}_3 + h\mathbf{k}_3 \tag{4}$$

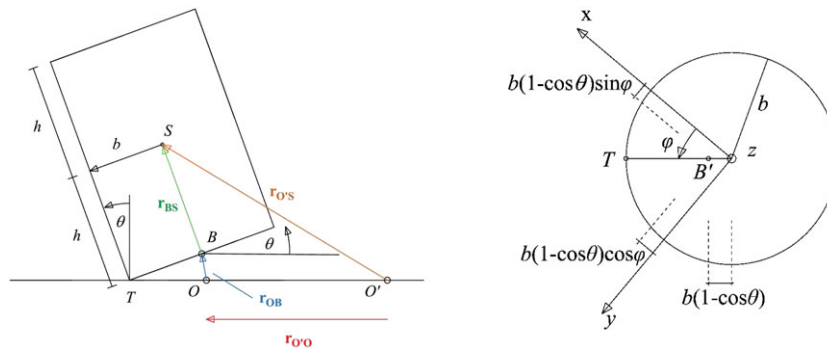


Figure 2. Left: vertical section passing through the center of mass of the rigid cylinder, S , and its contact point with the ground T , the pivot point. Right, top view: the circle is the original configuration of the cylinder and point B' is the vertical projection of point B on the ground. [Colour figure can be viewed at wileyonlinelibrary.com]

where \mathbf{i} , \mathbf{j} , and \mathbf{k} are the unit vectors of each coordinate system (with case and indexes corresponding to the notation of the corresponding axes) and u_{gx} and u_{gy} are the two horizontal components of the earthquake ground motion excitation. The unit vectors are related through the following transformations:

$$\begin{bmatrix} \mathbf{I} \\ \mathbf{J} \\ \mathbf{K} \end{bmatrix} = \mathbf{1} \cdot \begin{bmatrix} \mathbf{i} \\ \mathbf{j} \\ \mathbf{k} \end{bmatrix} \text{ and } \begin{bmatrix} \mathbf{i} \\ \mathbf{j} \\ \mathbf{k} \end{bmatrix} = \mathbf{A}_1 \cdot \mathbf{A}_2 \cdot \mathbf{A}_3 \cdot \begin{bmatrix} \mathbf{i}_3 \\ \mathbf{j}_3 \\ \mathbf{k}_3 \end{bmatrix} \quad (5)$$

where $\mathbf{1}$ is the unit matrix and \mathbf{A}_1 , \mathbf{A}_2 , and \mathbf{A}_3 are the rotation matrices that correspond to the Euler angles:

$$\mathbf{A}_1 = \begin{bmatrix} \cos\varphi & -\sin\varphi & 0 \\ \sin\varphi & \cos\varphi & 0 \\ 0 & 0 & 1 \end{bmatrix} \quad \mathbf{A}_2 = \begin{bmatrix} \cos\theta & 0 & \sin\theta \\ 0 & 1 & 0 \\ -\sin\theta & 0 & \cos\theta \end{bmatrix} \quad \mathbf{A}_3 = \begin{bmatrix} \cos\varphi & \sin\varphi & 0 \\ -\sin\varphi & \cos\varphi & 0 \\ 0 & 0 & 1 \end{bmatrix} \quad (6)$$

With reference to Equations (5) and (6), vector \mathbf{r}_{BS} can be written in XYZ coordinates as

$$\mathbf{r}_{BS} = h \cdot \cos\varphi \cdot \sin\theta \cdot \mathbf{I} + h \cdot \sin\varphi \cdot \sin\theta \cdot \mathbf{J} + h \cdot \cos\theta \cdot \mathbf{K} \quad (7)$$

or in vector coordinates as

$$\mathbf{r}_{BS} = h \begin{bmatrix} \cos\varphi \cdot \sin\theta \\ \sin\varphi \cdot \sin\theta \\ \cos\theta \end{bmatrix}_{XYZ} \quad (8)$$

With reference to Figure 2, d_x , d_y , and d_z from Equation (3) are

$$\begin{aligned} d_x &= b \cdot (1 - \cos\theta) \cdot \cos\varphi \\ d_y &= b \cdot (1 - \cos\theta) \cdot \sin\varphi \\ d_z &= b \cdot \sin\theta \end{aligned} \quad (9)$$

giving vector \mathbf{r}_{OB} :

$$\mathbf{r}_{OB} = b \cdot \begin{bmatrix} (1 - \cos\theta) \cdot \cos\varphi \\ (1 - \cos\theta) \cdot \sin\varphi \\ \sin\theta \end{bmatrix}_{XYZ} \quad (10)$$

Therefore, Equation (1) can be written in XYZ coordinates as

$$\mathbf{r}_{O'S} = \begin{bmatrix} u_{gx} \\ u_{gy} \\ 0 \end{bmatrix}_{XYZ} + b \cdot \begin{bmatrix} (1 - \cos\theta) \cdot \cos\varphi \\ (1 - \cos\theta) \cdot \sin\varphi \\ \sin\theta \end{bmatrix}_{XYZ} + h \begin{bmatrix} \cos\varphi \cdot \sin\theta \\ \sin\varphi \cdot \sin\theta \\ \cos\theta \end{bmatrix}_{XYZ} \quad (11)$$

2.2. Equations of motion

The Lagrangian equations of the rigid cylinder in Figure 1 are

$$\frac{d}{dt} \left(\frac{\partial(K - V)}{\partial \dot{q}_i} \right) - \frac{\partial(K - V)}{\partial q_i} = 0 \quad (12)$$

where q_i are the two degrees of freedom of the cylinder (θ and φ), while K and V are the kinetic and potential energy of the system, respectively. The translational kinetic energy of the system is

$$K_{\text{trans}} = \frac{1}{2} m \cdot \mathbf{r}_{O'S}^T \cdot \mathbf{r}_{O'S} \quad (13)$$

The angular velocity of the cylinder, in the $x_3y_3z_3$ coordinates, is [62]

$$\boldsymbol{\omega} = \begin{bmatrix} -\dot{\varphi} \cdot \cos\varphi \sin\theta - \dot{\theta} \cdot \sin\varphi \\ -\dot{\varphi} \cdot \sin\varphi \sin\theta + \dot{\theta} \cdot \cos\varphi \\ \dot{\varphi} \cdot \cos\theta - \dot{\theta} \end{bmatrix}_{x_3y_3z_3} \quad (14)$$

The rotational kinetic energy of the system is

$$K_{\text{rot}} = \frac{1}{2} \boldsymbol{\omega}^T \cdot \mathbf{I}_0 \cdot \boldsymbol{\omega} \quad (15)$$

where \mathbf{I}_0 is the moment of inertia tensor of the cylinder around its principal axis:

$$\mathbf{I}_0 = \begin{bmatrix} I_x & 0 & 0 \\ 0 & I_y & 0 \\ 0 & 0 & I_z \end{bmatrix} = \begin{bmatrix} \frac{3mb^2 + 4mh^2}{12} & 0 & 0 \\ 0 & \frac{3mb^2 + 4mh^2}{12} & 0 \\ 0 & 0 & \frac{mb^2}{2} \end{bmatrix} \quad (16)$$

The potential energy V of the system is

$$V = mg(b \sin\theta + h \cos\theta) \quad (17)$$

Equations (10) through (17) give the equations of motion or the rigid cylinder (Figure 1):

$$\begin{aligned} & (I_1 + h^2m + b^2m) \cdot \ddot{\theta} + bgm \cdot \cos\theta - hgm \cdot \sin\theta \\ & + ((I_2 - I_1 + b^2m - h^2m) \cdot \cos\theta \cdot \sin\theta - (I_2 + b^2m) \cdot \sin\theta - hbm \cdot (1 + \cos\theta) + 2hbm \cdot \cos^2\theta) \cdot \dot{\varphi}^2 = \\ & = -hm \cdot \ddot{u}_{gx} \cdot \cos\varphi \cdot \cos\theta - bm \cdot \ddot{u}_{gx} \cdot \cos\varphi \cdot \sin\theta - hm \cdot \ddot{u}_{gy} \cdot \sin\varphi \cdot \cos\theta - bm \cdot \ddot{u}_{gy} \cdot \sin\varphi \cdot \sin\theta \end{aligned} \quad (18)$$

$$\begin{aligned} & ((I_1 - I_2 + h^2m - b^2m) \cdot \sin^2\theta + 2 \cdot (I_2 + b^2m) \cdot (1 - \cos\theta) + 2hbm \cdot \sin\theta \cdot (1 - \cos\theta)) \cdot \ddot{\varphi} + \\ & (2 \cdot (I_2 - I_1 - h^2m + b^2m) \cdot \sin\theta \cdot (1 - \cos\theta) + 2hbm \cdot (2\sin^2\theta + \cos\theta - 1) + 2 \cdot (I_1 + h^2m) \cdot \sin\theta) \cdot \dot{\varphi} \cdot \dot{\theta} = \\ & = -bm \cdot \ddot{u}_{gx} \cdot (1 - \cos\theta) \cos\varphi + bm \cdot \ddot{u}_{gx} \cdot \sin\varphi \cdot (1 - \cos\theta) - hm \cdot \ddot{u}_{gy} \cdot \sin\theta \cos\varphi + hm \cdot \ddot{u}_{gy} \cdot \sin\varphi \cdot \sin\theta \end{aligned} \quad (19)$$

where I_1 is I_x and I_2 is I_z . Using Equation (16) and defining

$$R = \sqrt{h^2 + b^2} \quad (20)$$

Equations (18) and (19) become

$$\begin{aligned} \ddot{\theta} = & -p^2 \left(\sin(\alpha - \theta) + \cos(\alpha - \theta) \left(\cos\varphi \frac{\ddot{u}_{gx}}{g} + \sin\varphi \frac{\ddot{u}_{gy}}{g} \right) \right) \\ & - \left(\left(\frac{5}{4} \sin^2 \alpha - \frac{4}{3} \cos^2 \alpha \right) \cdot \cos\theta \cdot \sin\theta - \frac{3}{2} \sin^2 \alpha \cdot \sin\theta - \right. \\ & \left. - \cos\alpha \cdot \sin\alpha \cdot (1 + \cos\theta) + 2 \cos\alpha \cdot \sin\alpha \cdot \cos^2 \theta \right) \frac{1}{\left(\frac{5}{4} + \frac{1}{12} \cos^2 \alpha \right)} \dot{\varphi}^2 \end{aligned} \quad (21)$$

$$\begin{aligned} & \left(\frac{1}{12} (3 - 18 \sin^2 \alpha + 13 \cos^2 \alpha) \cdot \sin^2 \theta + 3 \sin^2 \alpha (1 - \cos\theta) + 2 \sin\alpha \cos\alpha \sin\theta \cdot (1 - \cos\theta) \right) R \cdot \dot{\varphi} + \\ & \left(3 \sin^2 \alpha \sin\theta + \frac{1}{6} (3 - 18 \sin^2 \alpha + 13 \cos^2 \alpha) \sin\theta \cos\theta + 2 \cos\alpha \sin\alpha (2 \sin^2 \theta + \cos\theta - 1) \right) R \cdot \dot{\varphi} \cdot \dot{\theta} = \\ & = (\sin\alpha + \sin(\theta - \alpha)) (\ddot{u}_{gx} \sin\varphi - \ddot{u}_{gy} \cos\varphi) \end{aligned} \quad (22)$$

where p is the well-known frequency parameter used in the dynamic model of the 2D rocking block, here associated with the tilting motion of the cylinder:

$$p^2 = \frac{mgR}{I_o} = \frac{12}{15 + \cos^2 \alpha} \frac{g}{R} \quad (23)$$

where I_o is the moment of inertia of the cylinder around a point on the circumference of its base. By setting $\dot{\varphi} = 0$ in Equation (21) and using single-horizontal-component ground excitation, one recovers the equation of the 2D rocking motion of a cylinder. However, unlike the equations used to describe the 2D rocking problem (which are non-smooth as they have to treat impact), the equations presented herein are smooth: the tilt angle θ is always positive, and the change of contact point is a continuous function of the rolling angle φ . There is no instantaneous impact, but the numerical results presented in the following sections show that a very rapid (but continuous) change of the pivot point may occur.

To solve the equations of motion (Equations (21) and (22)) numerically, 3D rocking-and-wobbling motion has to be initiated: in the case of free vibration, via a non-zero initial spin, $\dot{\varphi}$, and in the case of an earthquake excitation, via applying a two-horizontal-component ground excitation. Such initiation resembles numerical analysis of buckling using a second-order geometry method, where one needs to apply an initial imperfection in order to observe buckling.

Using Equation (21) without the ground motion excitation and assuming a constant cylinder tilt angle θ , one obtains the wobbling period of the cylinder as a function of the title angle θ :

$$T = \frac{2\pi}{p} \sqrt{\frac{\left(\left(\frac{5}{4} \sin^2 \alpha - \frac{4}{3} \cos^2 \alpha \right) \cdot \cos\theta \cdot \sin\theta - \frac{3}{2} \sin^2 \alpha \cdot \sin\theta - \right.}{\sin(\alpha - \theta) \left(\frac{5}{4} + \frac{1}{12} \cos^2 \alpha \right)} \left. - \cos\alpha \cdot \sin\alpha \cdot (1 + \cos\theta) + 2 \cos\alpha \cdot \sin\alpha \cdot \cos^2 \theta \right)} \quad (24)$$

Figure 3 plots the cylinder wobbling period T , normalized with respect to the cylinder frequency parameter p (Equation (24)), against the normalized tilt angle of the cylinder for different values of cylinder slenderness $\tan\alpha$. The Euler's Disk case is represented by $\tan\alpha = 1000$. The normalized

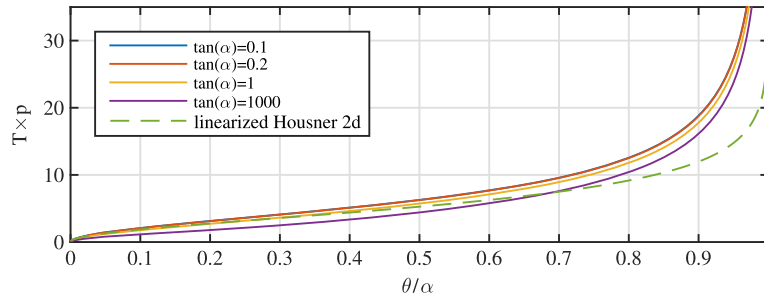


Figure 3. Period–tilt angle relation for rocking and wobbling cylinders of different slenderness. [Colour figure can be viewed at wileyonlinelibrary.com]

period of a 2D rocking block, as derived by Housner [3], is also plotted in Figure 3. The analogy between 2D rocking and 3D bounded wobbling is evident. Note that Housner’s derivation is linearized and holds only for small values of the slenderness angle α (then it is also independent of the exact value of α).

2.3. Uplift condition

Uplift occurs when the total ground acceleration is larger than $g \tan \alpha$:

$$\sqrt{\ddot{u}_{gx}^2 + \ddot{u}_{gy}^2} \geq g \tan \alpha \tag{25}$$

The direction of uplift is along the D’Alembert inertia force vector at the instance of uplift. This direction is given by the angle φ_0 :

$$\cos \varphi_0 = -\frac{u_{gx}}{\sqrt{\ddot{u}_{gx}^2 + \ddot{u}_{gy}^2}} \quad \text{and} \quad \sin \varphi_0 = -\frac{u_{gy}}{\sqrt{\ddot{u}_{gx}^2 + \ddot{u}_{gy}^2}} \tag{26}$$

2.4. Free vibration response

The aforementioned equations are implemented in MATLAB and solved numerically. Figure 4 plots three characteristic ($R = 6 \text{ m}$ and $\tan \alpha = 0.2$) rigid cylinder free rocking and wobbling motions from three initial conditions. The responses of the model without damping are plotted in black, but for the second and third cases, they are indistinguishable from the response of the damped model (see the next section). For a very small initial spin (Figure 4a and b), the cylinder changes its pivot point rapidly (but smoothly, as the solution is continuous). This is the quasi-rocking response mode. The term ‘quasi’ is used because this numerical test confirms the experimentally observed [44, 46] and theoretically proven result [47] that the planar motion of a cylinder is unstable: an initial angle of turn as low as $\dot{\varphi} = 10^{-8} \text{ rad/s}$ induces a clear out-of-plane motion. Therefore, the change of pivot point is defined by an angle of turn, slightly smaller than π , which compares well with the prediction of [48]. Indeed, [48] gives an angle of turn equal to

$$\Delta \varphi = \pi \sqrt{\frac{3 + 13 \cos^2 \alpha}{15 + \cos^2 \alpha}} = 3.0952 \tag{27}$$

while the numerical calculations give $\Delta \varphi = 3.058$.

The abrupt change of the pivot point generates large vertical forces at the contact point (in the limit case, they become infinite and the spinning motion tends to an impact). Therefore, one source of

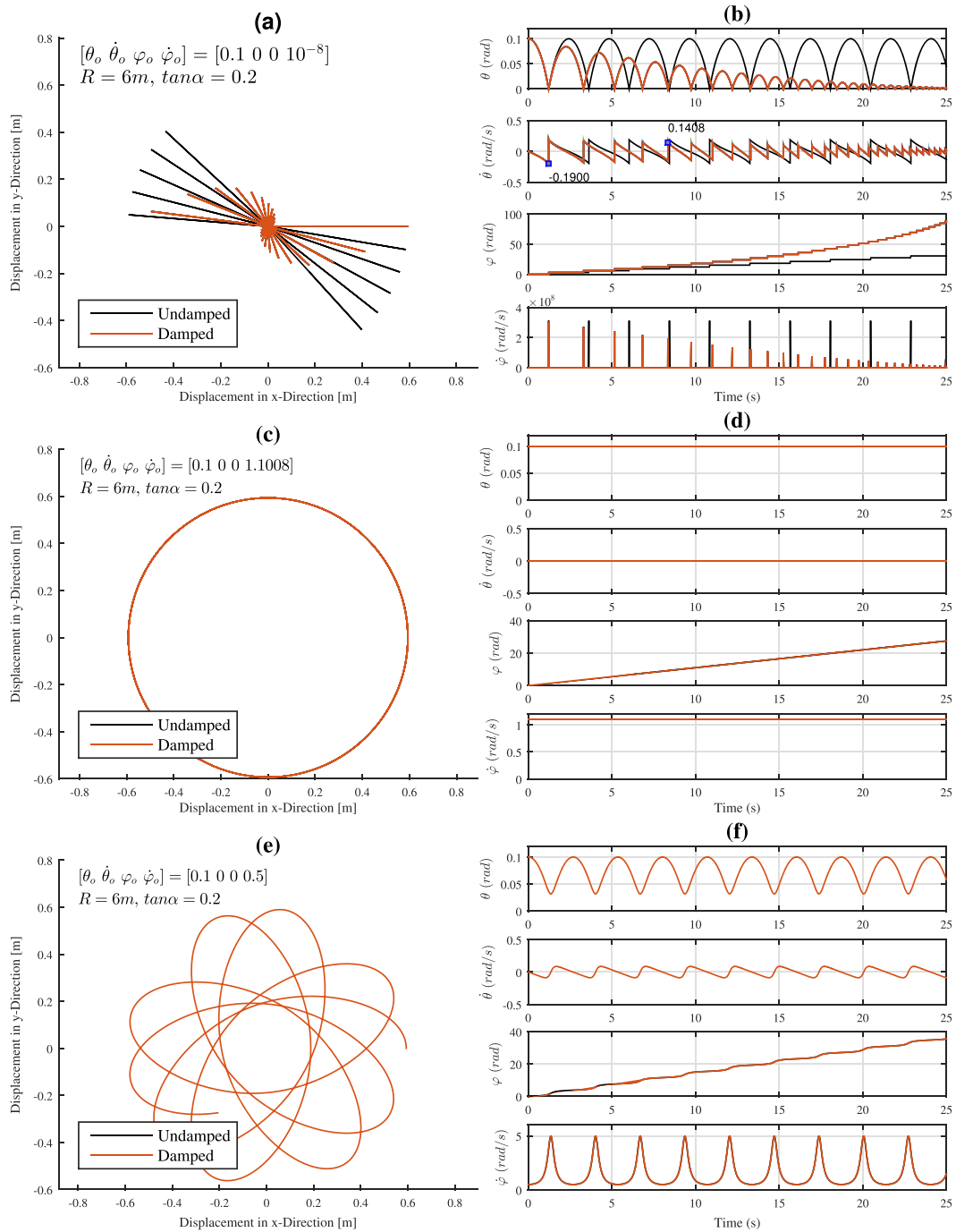


Figure 4. Left: orbits of the center of cylinder mass. Right: response time histories of the tilt magnitude and velocity θ , $\dot{\theta}$, and the spin magnitude and velocity φ and $\dot{\varphi}$ for free vibration with different initial conditions. [Colour figure can be viewed at wileyonlinelibrary.com]

damping of the rocking and wobbling motion of a rigid cylinder could be such a quasi-impact mechanism. This damping mechanism is introduced in the next section.

During the change of pivot point, a jump in the tilt velocity, $\dot{\theta}$, is observed. This is not a discontinuity (since the equations are smooth) but rather a rapid change of value. It does not appear in the 2D problem because in the 3D model θ is always positive and the change of pivot point does not happen by θ changing sign, but by a rapid change of φ .

Figure 4c and d plots the response of a rigid cylinder for an initial spin defined through Equation (24). For every cylinder geometry and each tilt angle, there exists a unique initial spin that can generate the response during which the tilt angle stays constant and the cylinder wobbles without rocking. This is the pure wobbling response mode. Note the much smaller magnitudes at the peak of the spin velocity, compared with the quasi-rocking response mode. It is also worth noting that since the tilt angle stays constant, the tilt acceleration, $\ddot{\theta}$, is zero, and hence, the vertical force at the contact point is constant and equal to the weight of the cylinder.

Figure 4e and f plots the response of a rigid cylinder due to a combination of the two pure response modes discussed earlier. Even though the two pure response modes interact, the tilt angle never comes close to zero. Note that the term ‘modes’ does not refer to modes of vibration resulting from modal analysis but rather identifies distinct types of rigid cylinder response.

3. DAMPED 3D BOUNDED MODEL OF A FREE-STANDING RIGID CYLINDER

Since the publication of Lord Rayleigh’s classic monograph ‘Theory of Sound’ [63], researchers have been using linear viscous dampers to model energy dissipation in structures. For MDOF systems, the damping matrix is often assumed to be mass and stiffness proportional, to facilitate uncoupled modal response analysis. This approach emerged from the necessity to model the decay of motion without having to solve systems of non-linear ODEs, which is oftentimes impossible to do analytically. Nowadays, the increase of computational power allows for the numerical solution of the equation of motion and, therefore, allows for the use of different energy dissipation models that might better describe the nature of the diminishing response of a moving structure. On the other hand, the use of Rayleigh damping to describe energy dissipation in rocking structures (2D or 3D) has been shown to be inadequate to describe the decay of the response and difficult to calibrate [[64] and references therein]. Therefore, Rayleigh damping is avoided, and a different method, based on [64], is suggested herein.

The energy dissipated by a rigid cylinder undergoing a pure wobbling motion on a rigid surface (Figure 4c and d) is very small. A spinning coin or the Euler’s Disk offers empirical proofs of this statement. There is an open debate on whether this energy dissipation originates from air viscosity [49] or friction [50], but there is a consensus that the amount of dissipated energy is small compared with the kinetic and potential energy quantities in the dynamic system. Furthermore, the cylinder remains in contact with the support, and the force at the contact point is constant and equal to the weight of the cylinder.

In the other extreme, in quasi-rocking motion (no spin $\dot{\varphi}$ and almost instantaneous change of pivot point), damping clearly exists. Unless there is a fracture of the surfaces in contact, energy dissipation is mainly due to radiation damping [65]. As Figure 4a and b shows, the contact force appears as a spike, quasi-impact, at every rapid change of the contact point. Furthermore, the closer the motion to pure rocking is, the larger the spike. In the limit case of instantaneous impact (Housner’s assumption for the 2D rocking problem), the impact force becomes a Dirac function. The variation of the contact force generates intense vibrations in the support (be it an infinite half-space or a real-world support) that lead to the gradual decay of motion.

If it is the variation of the contact force that causes energy to be dissipated from the rocking and wobbling rigid cylinder, it is reasonable to model this content using a linear spring in parallel with a linear viscous damper at the contact point (Figure 5). The viscous damper dissipates energy only when the contact point moves up and down and dissipates more energy when the point moves faster. It will be shown that the exact value of the damping coefficient for this damper is important only for free, quasi-rocking vibration, while knowing the exact damping coefficient value has marginal importance for modeling the response to earthquake ground motion excitation, especially when an intense excitation induces large-amplitude motion of the cylinder. Since the support is assumed to be rigid, the spring stiffness is set to a numerically very large value.

This model is not to be confused with Winkler springs: the contact is pointwise, and the spring and the dashpot are associated with the contact point, not distributed across the support surface. In a

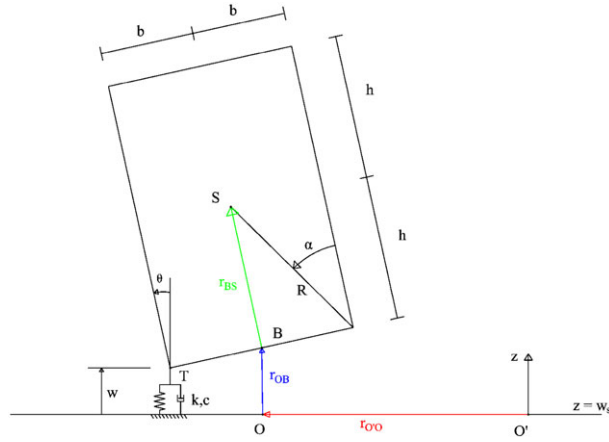


Figure 5. Model for energy dissipation (damping) at the contact point. [Colour figure can be viewed at wileyonlinelibrary.com]

Winkler model, the vertical force deformation response of the support is not linear, when the rocking body is uplifted, since more indentation of the body would mobilize more springs as the contact area increases to balance the actions of the body. Non-linear compression-only springs and contact point searches are avoided in the proposed model, making it much more computationally efficient, while not less realistic than a Winkler model given the assumption of support rigidity. Note that the spring and the dashpot are not used to describe the compressibility of the ground but are merely utilized to dissipate energy during the rolling and wobbling motion of the rigid cylinder on a rigid surface. The damped model (Figure 5) is described by the equations of motion

$$\begin{aligned} \ddot{\theta} = & -p^2 \left(\sin(\alpha - \theta) + \cos(\alpha - \theta) \left(\cos\phi \cdot \frac{\ddot{u}_{gx}}{g} + \sin\phi \cdot \frac{\ddot{u}_{gy}}{g} \right) \right) - \\ & - \frac{\dot{w}}{15 + \cos\alpha} \left(\sin(\alpha - \theta) + \cos(\alpha - \theta) \left(\cos\phi \cdot \frac{\ddot{u}_{gx}}{g} + \sin\phi \cdot \frac{\ddot{u}_{gy}}{g} \right) \right) \\ & - \left(\left(\frac{5}{4} \sin^2\alpha - \frac{4}{3} \cos^2\alpha \right) \cdot \cos\theta \cdot \sin\theta - \frac{3}{2} \sin^2\alpha \cdot \sin\theta - \right. \\ & \left. - \cos\alpha \cdot \sin\alpha \cdot (1 + \cos\theta) + 2 \cos\alpha \cdot \sin\alpha \cdot \cos^2\theta \right) \cdot \frac{1}{\left(\frac{5}{4} + \frac{1}{12} \cos^2\alpha \right)} \dot{\phi}^2 \end{aligned} \quad (28)$$

and

$$\dot{w} + 2\zeta\omega_n\dot{w} + \omega_n^2w = R \cos(\alpha - \theta)\dot{\theta}^2 - R \sin(\alpha - \theta)\ddot{\theta} \quad (29)$$

and by Equation (22), which remains unchanged. The properties of the spring and dashpot system are

$$\omega_n = \sqrt{\frac{k}{m}} \text{ and } \zeta = \frac{c}{2m\omega_n} = \frac{c}{c_{cr}} \quad (30)$$

Position $w = 0$ corresponds to a static equilibrium position of a titled cylinder, where the deformation of the contact point spring under the cylinder self-weight is equal to mg/k .

The free rocking and wobbling responses of undamped and damped ($R = 6$ m and $\tan\alpha = 0.2$) rigid cylinders from three initial conditions are compared in Figure 4. The responses are computed and plotted for eight combinations of spring and damper properties, namely, for $\omega_n = \{200, 2000\}$ rad/s and $\zeta = \{0.05, 0.5, 5, 50\}$. The plots overlap, indicating that the proposed 3D bounded rocking and

wobbling motion model is not sensitive to the values of the stiffness and damping parameters of the contact point spring and dashpot system (as long as the spring is stiff enough to represent a rigid support). This perhaps counterintuitive outcome is similar to the observations of 2D rocking response in [64] and is related to the fact that the impacts in rocking motion are not centric. Nevertheless, the proposed model succeeds in dissipating energy during motions that tend to pure rocking. In fact, Housner's approach for a rigid cylinder would give a coefficient of restitution equal to

$$\sqrt{r}_{Housner} = e = \frac{\dot{\theta}_{after}}{\dot{\theta}_{before}} = 1 - \frac{mR^2}{I_o} (1 - \cos 2\alpha) = 1 - \frac{\sin^2 \alpha}{\frac{5}{8} + \frac{1}{24} \cos^2 \alpha} = 0.942 \quad (31)$$

Calculating the coefficient of restitution from the first five impacts shown in Figure 4b yields

$$\sqrt{r}_{Numerical} = \left(\frac{0.1408}{0.19} \right)^{1/5} = 0.942 \quad (32)$$

The two values are equal to three significant digits. Therefore, the response of the 3D bounded rocking cylinder is not sensitive to the exact values of the spring and damper properties of the damped model even when the response involves quasi-impacts and virtually instantaneous changes of the contact point.

In the cases where the change of pivot point is not quasi-instantaneous (Figure 4c–f), there is zero damping and the damped and undamped models have the exact same response.

4. GROUND MOTION RESPONSE OF A FREE-STANDING RIGID CYLINDER

When the analysis of the undamped and damped free rocking and wobbling response of a free-standing 3D bounded rigid cylinder is extended, the response of the two models (damped and undamped) to earthquake excitation is going to be similar if wobbling motion dominates the response (i.e., quasi-impacts do not occur, and the amount of dissipated energy is very small). If, however, quasi-impacts occur, the damped model is going to dissipate non-negligible amounts of energy and the solutions from the two models will start to diverge.

To test the aforementioned statement, the support surface of a rigid cylinder with $R = 6$ m and $\tan \alpha = 0.2$ is excited bidirectionally using the two horizontal components of the 1940 Imperial Valley, El Centro ground motion record, baseline corrected via a high-pass filter (based on Brune's source model [66]). Moreover, the two original components are rotated to determine the two uncorrelated principal components [67, 68] (for reasons that will become clear in the next section). The two components are shown in the bottom two rows of Figure 6. The x -direction excitation is the EW component, and the y -direction excitation is the NS component of this motion, using the coordinate system shown in Figure 1. Indeed, for the first 15 s of the response, the undamped and damped solutions coincide. Then, a quasi-impact occurs, and the two solutions start to diverge. The divergence is evident in the time history of the rolling angle φ , as the two models spin in opposite directions; that is, the rolling angular velocities $\dot{\varphi}$ have opposite signs. However, up until the 19th second of motion, the difference is barely visible in the time history of the tilt angle θ . Interestingly, after 28 s, the two models spin in opposite directions; that is, the turn angles $\dot{\varphi}$ have opposite signs. The damped and undamped models produce maximum tilt angles θ equal to 0.0668 and 0.0838 rad, respectively, a 25% difference. Given all model approximations and uncertainties, this difference is small but not negligible. However, a comparison of the undamped and damped 3D rigid cylinder rolling and wobbling models using a single ground motion is not the most meaningful one: a more meaningful comparison is one obtained from the statistics of the response of the two models to an ensemble of ground motion that represent the same hazard. To this end, the so-called seismic rocking response spectra are presented in the following section.

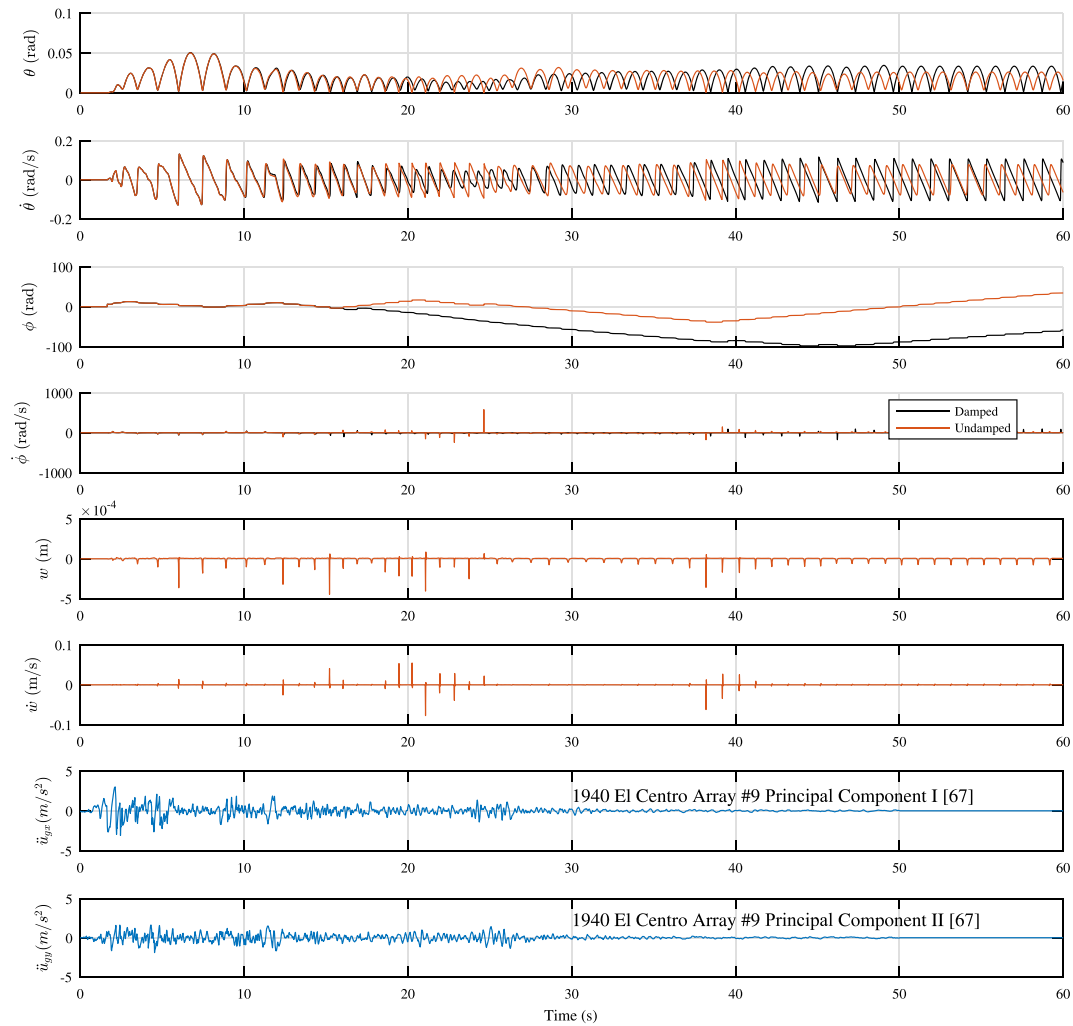


Figure 6. Rigid cylinder tilt θ , $\dot{\theta}$, spin ϕ , and $\dot{\phi}$ and spring displacement w and velocity \dot{w} response time histories to the 1940 El Centro ground motion (bottom two rows). [Colour figure can be viewed at wileyonlinelibrary.com]

5. SEISMIC PERFORMANCE ROCKING SPECTRA

In order to gain insight into the stability of rigid cylinders of different sizes under earthquake ground motion excitation, rocking response spectra are constructed by scaling the 1940 El Centro ground motion. Figure 7 plots the overturning spectra of El Centro ground motion (i.e., contour plots of maximum tilt angle, θ), for a given cylinder slenderness $\tan\alpha = 0.2$ computed using the undamped (left) and damped (right) models. The abscissa defines the size of the rigid cylinder through its semidiagonal, R . The ordinate defines the normalized peak ground acceleration, $PGA/g\tan\alpha$, where $PGA = \max\left(\sqrt{u_{gx}^2 + u_{gy}^2}\right)$. The main characteristic of rocking structures, in which for a given slenderness, larger structures are harder to overturn, still holds. The damped and undamped models give almost identical overturning spectra. Both components of the 1940 El Centro ground motion record were scaled equally. Furthermore, the scale factors needed to overturn large cylinders were large. Such scaling of a single recorded ground motion is not ideal as it may produce unrealistic, strong ground motions. Nevertheless, the present pilot study adopts this scaling model.

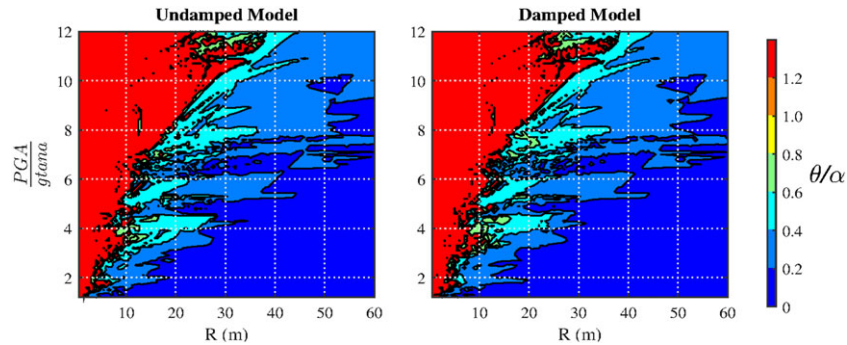


Figure 7. Normalized tilt angle θ/α contour plots for different cylinder sizes, R , and for the normalized scaled 1940 El Centro ground motion intensity $PGA/g\tan\alpha \cdot \tan\alpha = 0.2$. [Colour figure can be viewed at wileyonlinelibrary.com]

5.1. Ensemble of ground motions

Following the pioneer work of Yim *et al.* [4], the problem was studied using an ensemble of ground motions, rather than a single one. The Rezaeian and Der Kiureghian [68–70] stochastic ground motion model was used to create 10 ground motion records that have the same statistical properties as the 1940 El Centro ground motion. In order for the model to be applicable, the original El Centro ground motion was rotated by 22.33° so that its two components are uncorrelated. Figure 8 shows the acceleration traces in the two orthogonal horizontal directions as well as the elastic pseudo-acceleration response spectra of the generated artificial ground motion records. The top plot is the original corrected El Centro ground motion, while the next 10 are the simulated ones. Note that the simulated ground motions merely match the original ground motion in terms of selected response quantities of a *linear elastic* single-degree-of-freedom oscillator. This does not guarantee that non-linear or inelastic structures, such as rocking structures, will have similar responses to individual ground motions in the generated ensemble.

5.2. Seismic rocking performance spectra

The 3D seismic response of a free-standing bounded rigid cylinder rocking and wobbling on a rigid surface is monitored using two performance limit states:

1. Overturning, identified numerically as $\theta > \pi/2$, and
2. Excessive tilting, identified as the first occurrence of the cylinder tilt angle θ exceeding one-third of the cylinder slenderness α , that is, $\theta > \alpha/3$.

For each ground motion of Figure 8 and each value of the semidiagonal R , a series of 3D rigid cylinder response analyses were carried out to identify the smallest normalized ground motion intensity $PGA/g\tan\alpha$ required to exceed a selected performance limit state of the rigid cylinder. The slenderness ratio of the cylinder was held constant ($\tan\alpha = 0.2$). The resulting line in the R - $PGA/g\tan\alpha$ plane (Figure 9) plots this minimum ground motion intensity, normalized by the cylinder aspect ratio, against the cylinder size (semidiagonal) R . The plots in Figure 9 show such seismic performance rocking spectra for the overturning (left) and excessive tilting (right) performance limit states for the Figure 8 ground motions computed using the undamped (solid lines) and damped (dashed lines) 3D rolling and wobbling rigid cylinder models. For each R , the mean (among the 11 ground motions) was also computed and is plotted using a thick black line. Figure 10 plots such mean spectra for seven performance goals.

The first observation is that the main property of rocking structures (for a given slenderness, the larger objects are harder to overturn dynamically) holds in the 3D case as well.

The second observation (Figure 9, left) is that the undamped and damped models produce essentially identical overturning seismic rocking performance spectra. The differences between the excessive tilt seismic performance rocking spectra (Figure 9, right) for the individual motions are small and practically vanish when the average spectra are compared. This indicates that the

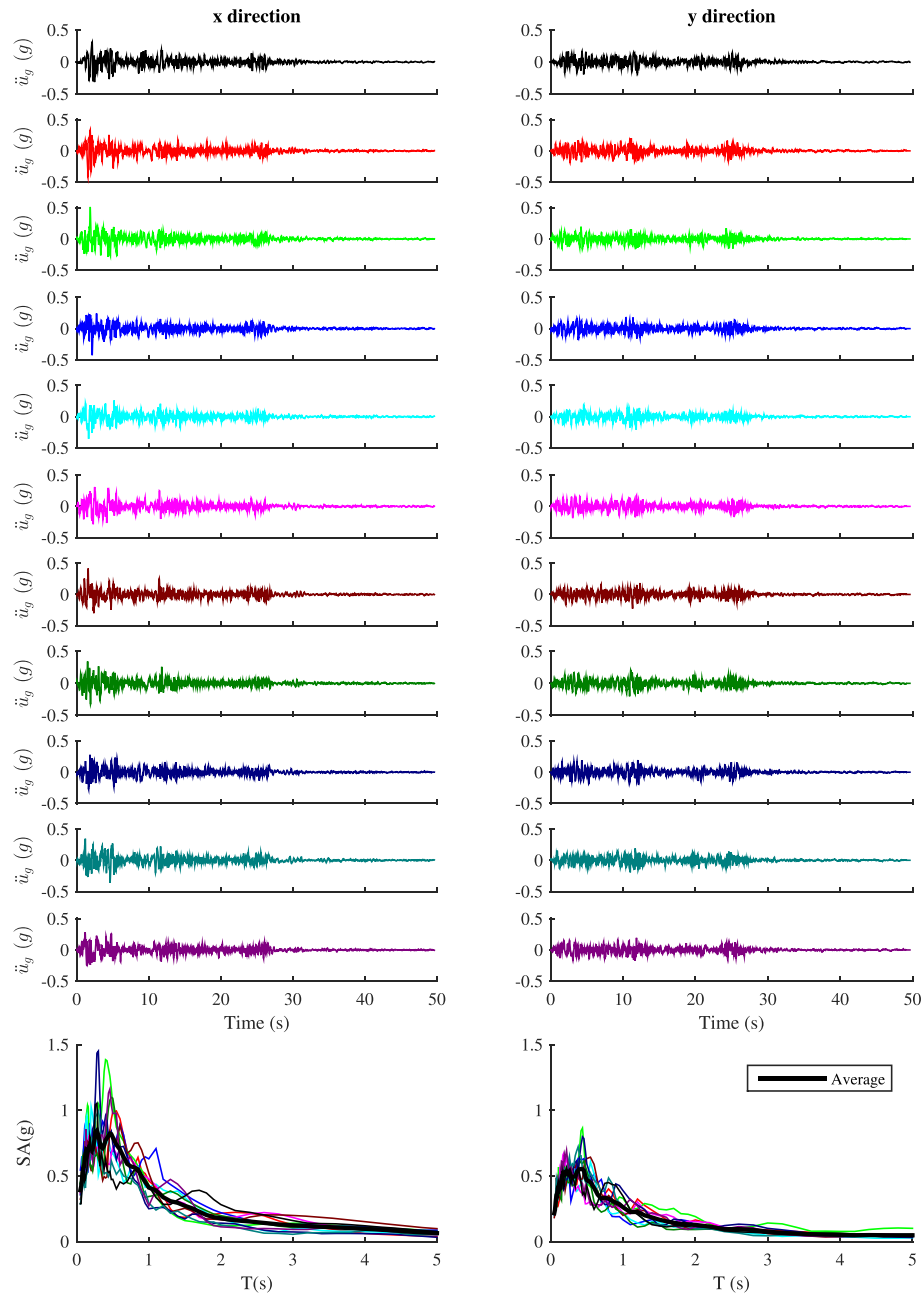


Figure 8. Acceleration traces in two orthogonal horizontal directions and the corresponding elastic pseudo-acceleration response spectra for the rotated 1940 El Centro ground motion (top) and the 10 generated artificial ground motion records that match the spectral characteristics of the rotated record. [Colour figure can be viewed at wileyonlinelibrary.com]

wobbling motion dominates the response of the rigid cylinder and that a few quasi-impacts that occur are not consequential enough to change the seismic performance spectra. Therefore, the exact value of the damping coefficient (associated with the viscous damper in the contact point damping model) is not important. Furthermore, the undamped 3D rigid cylinder model can be used to construct the seismic rocking performance spectra for 3D rocking and wobbling response of rigid cylinders with sufficient accuracy.

The third observation is that the average seismic performance rocking spectra for all performance limit states are almost straight lines, indicating that the average ground motion intensity to exceed a

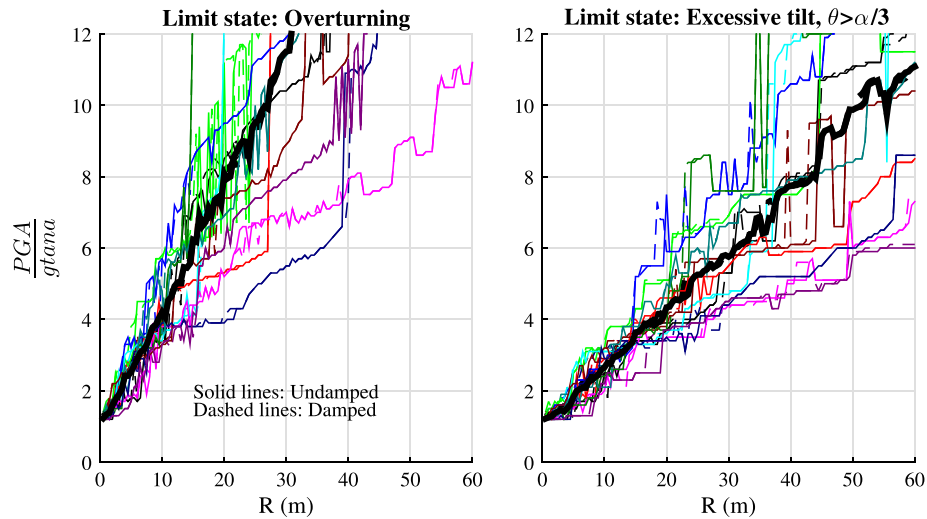


Figure 9. Seismic performance spectra for the three-dimensional rocking and wobbling bounded cylinder. Right: overturning performance limit state. Left: excessive tilting performance limit state. Spectra for the 11 individual ground motions shown in Figure 8 are drawn using the same colors. The thick black lines plot the average. [Colour figure can be viewed at wileyonlinelibrary.com]

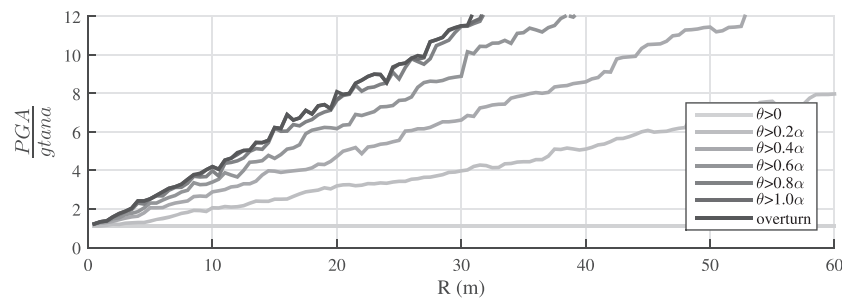


Figure 10. Seismic performance spectra for the three-dimensional rocking and wobbling bounded cylinder. Average (among all ground motions of Figure 8) of seismic performance rocking spectra. $\tan \alpha = 0.2$, undamped model.

cylinder performance limit state is linearly related to the size of the cylinder, at least for a set of broadband ground motions that are compatible with the El Centro 1940 ground motion. This is contrast with the overturning spectra for the analytical pulse ground motion excitation that exhibit a super-linear behavior; that is, the overturning acceleration grows exponentially with a linear increase of the rocking body size [6]. Nevertheless, this observation is of extraordinary importance as it may enable a straightforward seismic performance-based design of rocking and wobbling free-standing cylindrical structures. The slope of the spectrum will depend on the original ground motion, but a detailed study of this correlation lies beyond the scope of this paper.

Finally, it is evident that the artificially generated ground motion records with similar linear elastic oscillator response spectra do not have similar rocking spectra for the rigid cylinder. This is a strong indication that the statistical parameters that correlate well with the seismic response of single-degree-of-freedom oscillators with a linear and elastic restoring force are not representative of the seismic response of a free-standing rocking structure, whose restoring capability stems only from its own weight.

5.3. Influence of cylinder slenderness

Formal dimensional analysis for rocking structures excited by analytical pulse excitation shows that their response depends both on the normalized excitation intensity $PGA/gt \tan \alpha$ and on the rocking

body slenderness α [6]. Figure 11 plots the average seismic rocking performance spectra for rigid cylinders with slenderness ratios $\tan\alpha = 0.1, 0.2,$ and $0.3,$ computed using the ground motions in Figure 8 and the undamped 3D bounded rocking and wobbling rigid cylinder model. The spectra too do not match exactly, because slenderness α cannot be omitted from the set of dimensionless parameters that characterize the rocking problem but indicate that slenderness α (for a given $PGA/g\tan\alpha$) has a very small influence on the seismic performance of the rocking and wobbling rigid cylinder. Therefore, $PGA/g\tan\alpha$ and R are sufficient to describe the seismic performance (overturning or excessive tilting) of a rigid cylinder constrained to rock or wobble on its base circumference, when excited by a class of ground motion records that have the same elastic spectra characteristics as the 1940 El Centro ground motion record.

5.4. One-directional or bidirectional excitation

The 3D bounded rocking and wobbling model makes it possible to compare the bidirectional excitation response computed using both horizontal components of the ground motion record to the unidirectional responses computed using only one of the components. Namely, the same undamped 3D cylinder model with slenderness ratio $\tan\alpha = 0.2$ is excited using both ground motion components (bidirectional excitation) and using each component separately (unidirectional excitation). For consistency, PGA denotes the intensity of the bidirectional excitation computed as $\max\left(\sqrt{\ddot{u}_{gx}^2 + \ddot{u}_{gy}^2}\right),$ for all three models (3D and both 2D). The computed average seismic rocking performance spectra for the ground motion records shown in Figure 8 are presented in Figure 12 (in black). It is clear that larger cylinders require a more intense ground motion to exceed a

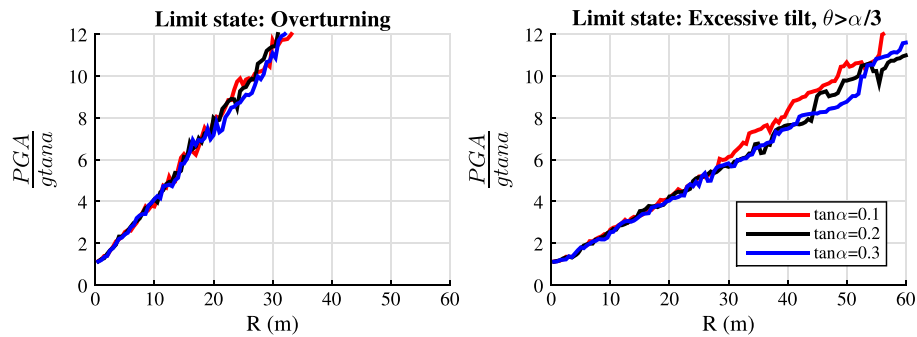


Figure 11. Average seismic performance rocking spectra for a rigid cylinder with different slenderness α . [Colour figure can be viewed at wileyonlinelibrary.com]

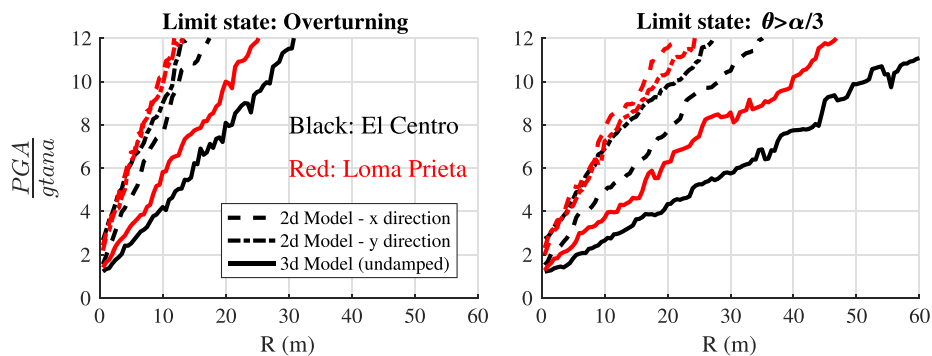


Figure 12. Average seismic performance rocking spectra for a rigid cylinder with slenderness ratio $\tan\alpha = 0.2$ computed using two-dimensional and three-dimensional ground motion excitations. [Colour figure can be viewed at wileyonlinelibrary.com]

performance limit state. However, overturning a cylinder with $R = 10$ m requires a bidirectional ground motion with intensity $PGA/\tan\alpha$ of about 4, while the intensities of unidirectional ground motion to overturn the same cylinder are twice as high. A similar trend holds for the excessive tilt performance limit state (Figure 12, right), as well as for a set of ground motions generated to match the San Jose–Santa Teresa Hills record of the Loma Prieta 1989 earthquake (Figure 12, red). Therefore, the outcomes of unidirectional seismic rocking performance analyses are grossly unconservative, strongly indicating that the seismic performance of free-standing cylindrical structures, such as ancient columns and chimneys, must be evaluated using bidirectional excitation. This finding is consistent with the results reported for all the other 3D ‘unbounded’ rocking models found in literature.

6. CONCLUSIONS

A two-degree-of-freedom model (three when damping is included) that describes the 3D dynamic behavior of a free-standing rigid cylindrical column that can uplift, rock, and wobble with the constraint that it does not slide or roll out of its original position (i.e., an inverted pendulum) was developed. It is the simplest 3D extension of the 2D Housner rigid-body rocking model. Two versions of the model were developed: an undamped one and a damped one. The latter is equipped with a damping mechanism such that the responses of a uniaxially excited 3D model and the 2D Housner model match well. It was found that the 3D motion of a free-standing rigid cylinder is dominated by wobbling, making the responses of the damped and undamped models essentially identical. Therefore, the simpler, undamped, model of the rocking and wobbling 3D motion of a bounded free-standing rigid cylinder can be used with confidence.

Seismic rocking performance spectra were constructed for the overturning and excessive tilting limit states and an ensemble of synthetic non-pulse-like ground motions that have similar elastic spectra to the 1940 El Centro and to the 1989 Loma Prieta ground motions. A comparison of the rigid cylinder responses computed using the proposed 3D model and a 2D rocking model shows that even though in both models the stability increases with block size (for a fixed slenderness), the 2D model is unconservative. It was also found that, for these ground motions, the mean PGA to reach a specific cylinder tilt angle increases almost linearly with cylinder size R . Therefore, the seismic rocking performance spectra have a very simple, linear, form. It was shown that the slenderness of the cylinder influences the seismic performance rocking spectra only through the non-dimensional parameter $PGA/g\tan\alpha$.

REFERENCES

1. Milne J. Seismic experiments. *Trans Seismological Society Japan* 1885; **8**:1–82.
2. Kirkpatrick P. Seismic measurements by the overthrow of columns. *Bulletin of the Seismological Society of America* 1927; **17**:95–109.
3. Housner GW. The behaviour of inverted pendulum structures during earthquakes. *Bulletin of the Seismological Society of America* 1963; **53**:404–417.
4. Yim CS, Chopra AK, Penzien J. Rocking response of rigid blocks to earthquakes. *Earthquake Engineering and Structural Dynamics* 1980; **8**:565–587.
5. Psycharis IN, Jennings PC. Rocking of slender rigid bodies allowed to uplift. *Earthquake Engineering and Structural Dynamics* 1983; **11**(1):57–76.
6. Zhang J, Makris N. Rocking response of free-standing blocks under cycloidal pulses. *Journal of Engineering Mechanics* 2001; **127**(5):473–483.
7. Makris N, Konstantinidis D. The rocking spectrum and the limitations of practical design methodologies. *Earthquake Engineering and Structural Dynamics* 2003; **32**(2):265–289.
8. Contento A, Di Egidio A. Investigations into the benefits of base isolation for non-symmetric rigid blocks. *Earthquake Engineering and Structural Dynamics* 2009; **38**(7):849–866.
9. Dimitrakopoulos EG, DeJong MJ. Revisiting the rocking block: closed-form solutions and similarity laws. *Proceedings Royal Society A: Mathematical, Physical and Engineering Science* 2012; **468**(2144):2294–2318.
10. Dimitrakopoulos EG, DeJong MJ. Overturning of retrofitted rocking structures under pulse-type excitations. *Journal of Engineering Mechanics* 2012; **138**(8):963–972.
11. Vassiliou MF, Makris N. Analysis of the rocking response of rigid blocks standing free on a seismically isolated base. *Earthquake Engineering and Structural Dynamics* 2012; **41**(2):177–196.

12. DeJong MJ, Dimitrakopoulos EG. Dynamically equivalent rocking structures. *Earthquake Engineering and Structural Dynamics* 2014; **43**(10):1543–1563.
13. Makris N. The role of the rotational inertia on the seismic resistance of free-standing rocking columns and articulated frames. *Bulletin of the Seismological Society of America* 2014; **104**(5):2226–2239.
14. Makris N. A half-century of rocking isolation. *Earthquakes Structures* 2014; **7**(6):1187–1221.
15. Makris N, Kampas G. Size versus slenderness: two competing parameters in the seismic stability of free-standing rocking columns. *Bulletin of the Seismological Society of America* 2016; **106**(1):104–122.
16. Makris N, Vassiliou MF. Sizing the slenderness of free-standing rocking columns to withstand earthquake shaking. *Archive of Applied Mechanics* 2012; **82**(10–11):1497–1511.
17. Oliveto G, Calò I, Greco A. Large displacement behaviour of a structural model with foundation uplift under impulsive and earthquake excitations. *Earthquake Engineering and Structural Dynamics* 2003; **32**(3):369–393.
18. Ma QTM, (2010): The mechanics of rocking structures subjected to ground motion (PhD dissertation, University of Auckland, NZ.)
19. Vassiliou MF, Mackie KR, Stojadinović B. Dynamic response analysis of solitary flexible rocking bodies: modeling and behavior under pulse-like ground excitation. *Earthquake Engineering and Structural Dynamics* 2014; **43**(10):1463–1481.
20. Acikgoz S, DeJong MJ. The rocking response of large flexible structures to earthquakes. *Bulletin of Earthquake Engineering* 2014; **12**(2):875–908.
21. Vassiliou MF, Truniger RE, Stojadinović B. An analytical model of a deformable cantilever structure rocking on a rigid surface: development and verification. *Earthquake Engineering and Structural Dynamics* 2015; **44**(13):2775–2794.
22. Konstantinidis D, Makris N. Seismic response analysis of multidrum classical columns. *Earthquake Engineering and Structural Dynamics* 2005; **34**(10):1243–1270.
23. Papalouzou L, Komodromos P. Planar investigation of the seismic response of ancient columns and colonnades with epistyles using a custom-made software. *Soil Dynamics and Earthquake Engineering* 2009; **29**(11–12):1437–1454.
24. Makris N, Vassiliou MF. Planar rocking response and stability analysis of an array of free-standing columns capped with a freely supported rigid beam. *Earthquake Engineering and Structural Dynamics* 2013; **42**(3):431–449.
25. Makris N, Vassiliou MF. Are some top-heavy structures more stable? *Journal of Structural Engineering* 2014; **140**(5):06014001.
26. Dimitrakopoulos EG, Giouvanidis AI. Seismic response analysis of the planar rocking frame. *Journal of Engineering Mechanics* 2015; **141**(7):04015003.
27. Makris N, Vassiliou MF. The dynamics of the rocking frame. *Seismic Assessment, Behavior and Retrofit of Heritage Buildings and Monuments*. Springer International Publishing: Switzerland, 2015; 37–59.
28. Makris N, Vassiliou MF. Seismic response and stability of the rocking frame. *Computational Methods, Seismic Protection, Hybrid Testing and Resilience in Earthquake Engineering*. Springer International Publishing: Switzerland, 2015; 249–273.
29. Peña F, Prieto F, Lourenço PB, Campos Costa A, Lemos JV. On the dynamics of rocking motion of single rigid-block structures. *Earthquake Engineering and Structural Dynamics* 2007; **36**(15):2383–2399.
30. Truniger RE, Vassiliou MF, Stojadinović B. An analytical model of a deformable cantilever structure rocking on a rigid surface: experimental validation. *Earthquake Engineering and Structural Dynamics* 2015; **44**(13):2795–2815.
31. Bachmann JA, Blöchlinger P, Wellauer M, Vassiliou MF, and Stojadinović B (2016): Experimental investigation of the seismic response of a column rocking and rolling on a concave base ECCOMAS Congress 2016: 7th European Congress on Computational Methods in Applied Sciences and Engineering, 2016.
32. Psycharis IN, Fragiadakis M, Stefanou I. Seismic reliability assessment of classical columns subjected to near-fault ground motions. *Earthquake Engineering and Structural Dynamics* 2013; **42**(14):2061–2079.
33. Dimitrakopoulos EG, Paraskeva TS. Dimensionless fragility curves for rocking response to near-fault excitations. *Earthquake Engineering and Structural Dynamics* 2015; **44**(12):2015–2033.
34. Bakhtary E, Gardoni P. Probabilistic seismic demand model and fragility estimates for rocking symmetric blocks. *Engineering Structures* 2016; **114**:25–34.
35. Vassiliou MF, Makris N. Dynamics of the vertically restrained rocking column. *Journal of Engineering Mechanics* 2015; **141**(12):04015049.
36. Makris N, Vassiliou MF. Dynamics of the rocking frame with vertical restrainers. *Journal of Structural Engineering* 2015; **141**(10):04014245.
37. Dimitrakopoulos EG, De Jong MJ. Seismic overturning of rocking structures with external viscous dampers. *Computational Methods in Earthquake Engineering*. Springer International Publishing: Netherlands, 2013.
38. Koh AS, Mustafa G. Free rocking of cylindrical structures. *Journal of Engineering Mechanics* 1990; **116**(1):35–54.
39. Koh AS, Hsiung CM. Base isolation benefits of 3-D rocking and uplift. I: theory. *Journal of Engineering Mechanics* 1991; **117**(1):1–18.
40. Koh AS, Hsiung CM. Base isolation benefits of 3-D rocking and uplift. II: numerical example. *Journal of Engineering Mechanics* 1991; **117**(1):19–31.
41. Ambraseys N, Psycharis IN. Earthquake stability of columns and statues. *Journal of Earthquake Engineering* 2011; **15**(5):685–710.
42. Stefanou I, Psycharis I, Georgopoulos IO. Dynamic response of reinforced masonry columns in classical monuments. *Construction and Building Materials* 2011; **25**(12):4325–4337.
43. Krstevska, L., Mihailov, V., Boschi, E., & Rovelli, A. (1996). Experimental dynamic testing of prototype and model of the Antonina Column in Roma. Proceedings of the 11th World Conference on Earthquake Engineering (Paper No. 546).

44. Mouzakis HP, Psycharis IN, Papastamatiou DY, Carydis PG, Papantonopoulos C, Zambas C. Experimental investigation of the earthquake response of a model of a marble classical column. *Earthquake Engineering and Structural Dynamics* 2002; **31**(9):1681–1698.
45. Drosos V, Anastasopoulos I. Shaking table testing of multidrum columns and portals. *Earthquake Engineering and Structural Dynamics* 2014; **43**(11):1703–1723.
46. Makris N, Alexakis H, Kampas G, Strepelias I, Kolonas C and Bousias S (2015): Seismic protection of bridges with rocking piers which recenter with gravity, Report EEAM, 2015-01, Department of Civil Engineering, University of Patras
47. Stefanou I, Vardoulakis I, Mavraganis A. Dynamic motion of a conical frustum over a rough horizontal plane. *International Journal of Non-linear Mechanics* 2011; **46**(1):114–124.
48. Srinivasan M, Ruina A. Rocking and rolling: a can that appears to rock might actually roll. *Physical Review E* 2008; **78**(6):066609.
49. Moffatt HK. Euler's disk and its finite-time singularity. *Nature* 2000; **404**(6780):833–834.
50. van den Engh G, Nelson P, Roach J. Numismatic gyrations. *Nature* 2000; **408**(6812):540.
51. McDonald AJ, McDonald KT (2000). The rolling motion of a disk on a horizontal plane. Preprint Archive, Los Alamos National Laboratory. arXiv: physics/008227.
52. Moffatt HK. Reply to 'numismatic gyrations'. *Nature* 2000; **408**(6812):540.
53. Kessler P, O'Reilly OM. The ringing of Euler's disk. *Regular and Chaotic dynamics* 2002; **7**(1):49–60.
54. Konstantinidis D and Makris N (2007): The dynamics of a rocking block in three dimensions, 8th Hell. Soc. Theor. Appl. Mech. Int. Congr. Mech. Patras, Greece 9/2015.
55. Zulli D, Contento A, Di Egidio A. 3D model of rigid block with a rectangular base subject to pulse-type excitation. *International Journal of Non-linear Mechanics* 2102; **47**(6):679–687.
56. Chatzis, MN and Smyth AW. Modeling of the 3D rocking problem. *International Journal of Non-linear Mechanics* 2012; **47**(4):85–98.
57. Chatzis MN, Smyth AW. Three-dimensional dynamics of a rigid body with wheels on a moving base. *Journal of Engineering Mechanics* 2012; **139**(4):496–511.
58. Greenbaum RJ, Smyth AW, Chatzis MN. Monocular computer vision method for the experimental study of three-dimensional rocking motion. *Journal of Engineering Mechanics* 2015; **142**(1):04015062.
59. Mathey C, Feau C, Politopoulos I, Clair D, Baillet L, Fogli M. Behavior of rigid blocks with geometrical defects under seismic motion: an experimental and numerical study. *Earthquake Engineering and Structural Dynamics* 2016; **45**(15):2413–2588.
60. Pappas A, Sextos A, da Porto F, Modena C. Efficiency of alternative intensity measures for the seismic assessment of monolithic free-standing columns. *Bull Earthquake Eng* 2016. <https://doi.org/10.1007/s10518-016-0035-0>.
61. Mashal M, Palermo A, Experimental testing of emulative and post-tensioned earthquake damage resistant technologies for accelerated bridge construction, Proceedings of the 16th World Conference on Earthquake Engineering, 16WCEE 2017, Santiago, Chile, January 9 to 13, 2017.
62. Ginsberg JH. *Advanced Engineering Dynamics*. Cambridge University Press: Cambridge, 1998.
63. Rayleigh L. *The Theory of Sound*. MacMillan and Company Ltd.: London, 1877.
64. Vassiliou MF, Mackie KR, Stojadinović B. A finite element model for seismic response analysis of deformable rocking frames. *Earthquake Engineering and Structural Dynamics* 2016. <https://doi.org/10.1002/eqe.2799>.
65. Adamidis O, Gazetas G, Anastasopoulos I, Argyrou C. Equivalent-linear stiffness and damping in rocking of circular and strip foundations. *Bulletin of Earthquake Engineering*, **12**(3):1177–1200.
66. Brune JN. Tectonic stress and the spectra of seismic shear waves from earthquakes. *Journal of Geophysical Research* 1970; **75**:4997–5009.
67. Penzien J, Watabe M. Characteristics of 3-dimensional earthquake ground motions. *Earthquake Engineering and Structural Dynamics* 1975; **3**:365–373.
68. Rezaeian S, Der Kiureghian A. Simulation of orthogonal horizontal ground motion components for specified earthquake and site characteristics. *Earthquake Engineering and Structural Dynamics* 2012; **41**:335–353.
69. Rezaeian S, Der Kiureghian A. A stochastic ground motion model with separable temporal and spectral nonstationarities. *Earthquake Engineering and Structural Dynamics* 2008; **37**(13):1565–1584.
70. Broccardo, M., & Der Kiureghian, A. (2014). Simulation of near-fault ground motions using frequency-domain discretization. In Proceedings of the 10th National Conference on Earthquake Engineering, Anchorage, Alaska.